Polymer Journal (2012) 44, 240–244

www.nature.com/pj

ORIGINAL ARTICLE

Dependence of the swelling behavior of a pH-responsive PEG-modified nanogel on the cross-link density

Goshu Tamura[1,2], Yuya Shinohara[1,2], Atsushi Tamura[3,6], Yusuke Sanada[2,4], Motoi Oishi[3], Isamu Akiba[2,4], Yukio Nagasaki[3,5], Kazuo Sakurai[2,4] and Yoshiyuki Amemiya[1,2]

We report pH-responsive structural changes in PEG-modified (PEGylated) nanogels, as determined by using small-angle X-ray scattering and dynamic light scattering. The size of the nanogels discontinuously increased at a lower pH than the pK_a of the nanogels. This size increase was attributed to the swelling of the core part of the nanogel upon a change in pH. The swelling behavior was dependent on the cross-link density of the core. When the cross-link density was low, the core swelled greatly with preserving the polydispersity in size and maintained a constant shape; however, when the cross-link density was high, the core swelled minimally, and only the polydispersity increased. This difference in swelling behavior is discussed in terms of the inhomogeneous structural distribution of cross-links in the core.
Polymer Journal (2012) **44,** 240–244; doi:10.1038/pj.2011.123; published online 23 November 2011

Keywords: drug delivery system; PEGylated nanogel; pH-responsive swelling; small-angle X-ray scattering

INTRODUCTION

Nanoparticle-based drug delivery systems, including liposomes, polymeric micelles and other nanoparticles, have received growing attention with respect to their clinical application to cancer chemotherapy. These formulations improve therapeutic efficacy while mitigating the severity of the side effects of tumoricidal payloads, through altering the drug's pharmacokinetics and pharmacodynamics.[1–4] Because the bio-distribution of intravenously administered nanoparticles is largely dependent on their size and surface properties, numerous surface modification techniques have been developed to regulate distribution within the body for therapeutic treatment.[5–7] In this regard, poly(ethylene glycol) (PEG) modification by the covalent coupling of hydrophilic PEG to pharmaceutical materials, often referred to as 'PEGylation,' represents a crucial strategy for prolonging the blood circulation time of delivery vehicles; densely grafted PEG-tethered chains minimize nonspecific interactions with serum proteins and the endothelia that line the blood vessels, through entropic repulsion.[8] This technology was developed from pioneering work on the chemical attachment of PEG to proteins,[9] and its efficacy has been demonstrated for polymeric micelles constructed from PEG hydrophobic block copolymers,[10] for which the hydrophobic chains aggregate to form a spherical core domain in aqueous solutions. Sterically stabilized PEG-modified (PEGylated) nanoparticles, such as stealth liposomes and core-shell polymeric micelles, can escape recognition by immune system responses, such as those of the reticuloendothelial system, resulting in long blood circulation times and preferential accumulation in tumor tissues through the enhanced permeability and retention effect.[11,12] To further enhance the therapeutic efficacy in targeted tissues, as well as to reduce the side effects in normal tissues, the selective release of therapeutic payloads in response to external stimuli, such as pH, temperature, light irradiation, and reaction with specific molecules or enzymes, is employed via drug nanocarriers. Among various external stimuli, pH is of greatest interest because a drastic decrease in pH is known to occur in various tissues and organelles such as endosomes/lysosomes, extra-tumoral environments, and inflamed regions, where the pH is lower than that of normal tissue and the blood stream (which have a pH $\sim$7.4);[13–16] thus, the development of pH-responsive drug nanocarriers should be an effective strategy to facilitate the clinical use of nanocarrier-based drug delivery systems.

Nagasaki *et al.* have developed core-shell-structured and pH-responsive PEGylated nanogel particles consisting of a cross-linked poly[2-(*N*,*N*-diethylaminoethyl) methacrylate] gel and tethered PEG chains.[17–22] These nanogel particles may be applicable not only for drug delivery systems but also for various therapeutics and pathog-

[1]Department of Advanced Materials Science, Graduate School of Frontier Sciences, University of Tokyo, Kashiwa, Chiba, Japan; [2]Japan Science and Technology Agency (JST) CREST, Chiyoda, Tokyo, Japan; [3]Department of Materials Science, Graduate School of Pure and Applied Sciences, University of Tsukuba, Tsukuba, Ibaraki, Japan; [4]Department of Chemistry and Biochemistry, University of Kitakyushu, Kitakyusyu, Fukuoka, Japan and [5]Satellite Laboratory of International Center for Materials Nanoarchitechtonics, National Institute for Materials Science, University of Tsukuba, Tsukuba, Ibaraki, Japan
[6]Present address: Institute of Advanced Biomedical Engineering and Science, Tokyo Women's Medical University.
Correspondence: Dr Y Shinohara, Department of Advanced Materials Science, Graduate School of Frontier Sciences, University of Tokyo, 5-1-5 Kashiwanoha, Kashiwa, Chiba 277-8561, Japan.
E-mail: yuya@k.u-tokyo.ac.jp
Received 26 May 2011; revised 31 August 2011; accepted 9 October 2011; published online 23 November 2011

nomony, such as small interfering RNA delivery, cancer photothermal therapy, magnetic resonance imaging and apoptosis probes, that are used to monitor responses to cancer therapy. For all of these applications, the poly[2-(*N*,*N*-diethylaminoethyl) methacrylate] gel core of the nanogels acts as a reservoir for anticancer drugs, small interfering RNAs, and metal nanoparticles through hydrophobic interactions, electrostatic interactions and coordination bonds with poly[2-(*N*,*N*-diethylaminoethyl) methacrylate] segments. The therapeutic effects of these nanogel derivatives have been well demonstrated,[22] but the detailed structural changes that occur upon the release of drugs, for example, have not yet been clarified.

In the present study, we sought to investigate the detailed pH-dependent structural changes in a PEGylated nanogel. In previous studies, pH-dependent changes in the hydrodynamic radius of nanogel particles were visualized with dynamic light scattering (DLS);[17–22] the size of nanogel particles increases under acidic conditions and decreases under alkaline conditions. Although DLS is widely used to characterize particle size and size distribution, estimates using DLS are often affected by many factors, including particle shape and surface structure, as discussed in Results and discussion. To characterize the detailed structure of the nanogel studied herein, particularly its core, we utilized small-angle X-ray scattering (SAXS) and DLS. SAXS is a powerful technique used to determine the structure of soft materials and has been successfully applied to determine the structure of core-shell shaped polymeric micelles.[23–28] In this paper, we first describe the pH-dependent swelling behavior of the PEGylated nanogel and then demonstrate the dependence of pH-responsive swelling on the cross-link density of PEGylated nanogels.

MATERIALS AND METHODS

Materials

PEGylated nanogels with different cross-link densities were synthesized by the emulsion copolymerization of 2-(*N*, *N*-(diethylamino)ethyl methacrylate (DEAMA; Wako, Japan), ethyleneglycol dimethacrylate (EGDMA; Wako, Japan), and heterobifunctional α-acetal-ω-vinylbenzyl-PEG macromonomer (acetal-PEG-VB)[22] in the presence of potassium persulfate (KPS; Wako, Japan) as an initiator. The details of the synthesis procedure are described elsewhere.[17–22] The number-averaged molecular weight, M_n, and M_n/M_w of the acetal-PEG-VB were 7870 and 1.07, respectively, where M_w is the weight-averaged molecular weight. The PEGylated nanogels consisted of a DEAMA core and a shell composed of acetal-PEG-VB. The core chain was cross-linked by EGDMA monomers; thus, the amount of EGDAMA defined the cross-link density of the core. The molar ratio of DEAMA and acetal-PEG-VB was held constant at [DEAMA]: [acetal-PEG-VB]=98.8: 1.2 for all samples. The cross-link density of the nanogels was defined as the molar percentage of EGDMA to the sum of DEAMA and acetal-PEG-VB. The sample code is shown in Table 1. All samples were purified by ultrafiltration (cutoff molecular weight: 200 000, Advantec, Tokyo, Japan) using methanol to remove the unreacted starting reagents, followed by ultrafiltration using deionized and distilled water to replace the solvent. The obtained nanogel solution was used as a stock solution, the concentration of which was determined by weighing the sample before and after lyophilization.

The chemical composition of PEGylated nanogels was determined by CHN elemental analysis using a series II CHNS/O Analyzer 2400 (Perkin Elmer, Waltham, MA, USA). The results are shown in Table 2. The measured CHN compositions were consistent with the feed molar compositions, indicating that the PEGylated nanogels were synthesized as designed.

Titration measurement

The degree of protonation, α, and pK_a of the PEGylated nanogels were measured with potentiometric titration. The stock solutions of PEGylated nanogel (7.8 mg) were mixed with NaCl (23.4 mg) and 0.01 N HCL (6.0 ml); then, their volumes were adjusted to 40 ml using distilled water to produce a final NaCl concentration of 10 mM. This solution was titrated with 0.01 N NaOH containing 10 mM NaCl at using an automatic titrator (DL-25, Mettler-Toledo, Zurich, Switzerland) at 298 K. The titrant was added in quantities of 0.05 ml at intervals of 30 s. From the obtained titration curves and the molar amounts of sample and titration solution, pH-α curves were calculated.

Table 1 Sample code and the molar ratio of DEAMA, acetal-PEG-VB and EGDMA

	DEAMA	*Acetal-PEG-VB*	*EGDMA*
CD1	98.8	1.2	1
CD2	98.8	1.2	2
CD5	98.8	1.2	5

Table 2 Results of CHN analysis of PEGylated nanogels

	Feed			*Observed*		
	C [%]	*H [%]*	*N [%]*	*C [%]*	*H [%]*	*N [%]*
CD1	61.06	9.84	4.96	61.28	9.81	5.16
CD2	61.05	9.82	4.93	60.97	9.33	5.20
CD5	61.04	9.76	4.82	60.01	9.20	4.80

DLS measurement

The hydrodynamic radius (R_h) of the nanogel and its standard deviation (δR_h) were measured by DLS (Zetasizer Nano ZS, Malvern Instruments, Worcestershire, UK) equipped with a 4-mW He-Ne-ion laser (wavelength=633 nm). The DLS measurements were performed at 298 K at a detection angle of 173°, and the values of R_h and $\delta R_h/R_h$ were estimated with the cumulant method.[29] The sizes of the nanogels at a concentration of 100 μg/ml under various pH conditions were measured. The pH values of the gels were adjusted by adding 10 mM of TRIS (tris(hydroxymethyl)aminomethane) solution and 10 mM of TRIS-HCl (Trizma: tris(hydroxymethyl)aminomethane hydrochloride) solution.

SAXS measurement

SAXS measurements were performed at BL03XU[30] and BL45XU,[31] SPring-8 (Hyogo, Japan). An R-AXIS VII imaging plate detector (Rigaku, Tokyo, Japan) was used to record the scattered X-ray intensity $I(q)$ as a function of q. The scattering vector q is expressed in terms of the X-ray wavelength λ and the scattering angle 2θ as $q=4\pi/\lambda \sin\theta$. Two ion chambers located upstream and downstream of the sample were used to measure the X-ray transmittance of the sample. To reduce parasitic scattering, a specially designed vacuum chamber[27,32] was used. The solution samples were sonicated for 1 min using a homogenizer (UH-50, SMT, Tokyo, Japan) a few minutes before SAXS measurements; this procedure enabled us to effectively remove large aggregates that would have caused undesired noise in the scattering intensity profiles at low angles. Then, the samples were placed into a quartz capillary cell (φ=2.0 mm, Hilgenberg GmbH, Malsfeld, Germany) and sealed with an epoxy resin. The wavelengths, the sample-to-detector distances, and the exposure times were 0.090 and 0.15 nm, 4.0 and 3.5 m, and 30 and 300 s at the BL03XU and BL45XU, respectively. The value of q was calibrated by the diffraction peak of silver behenate.[32] To cover a wide q-range, the SAXS intensity profiles at the BL03XU ($0.02<q<0.1\ nm^{-1}$) and BL45XU ($0.05<q<1\ nm^{-1}$) were combined. All measurements were performed at room temperature.

RESULTS AND DISCUSSION

Protonation of nanogel upon pH change

Figure 1 shows the pH-α curves of the PEGylated nanogels. The degree of protonation of CD1, CD2 and CD5 at pH=8.0 was approximately zero. By contrast, the degree of protonation of CD1 and CD2 at

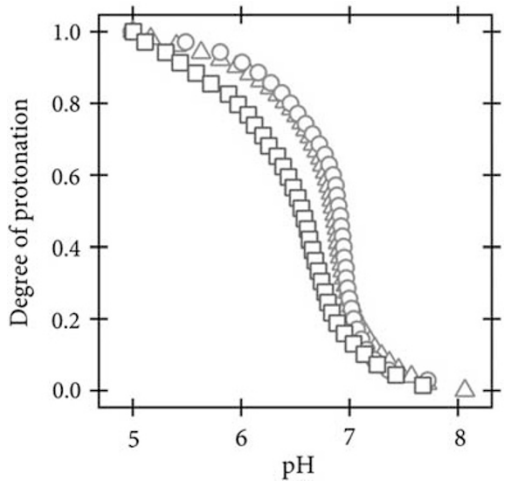

Figure 1 Dependence of degree of protonation on pH: CD1 (circles), CD2 (triangles), and CD5 (squares). A full color version of this figure is available at *Polymer Journal* online.

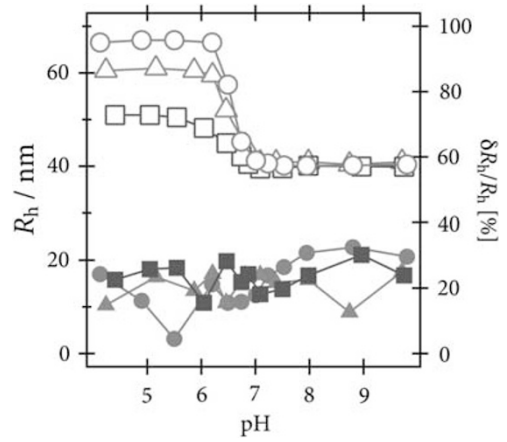

Figure 2 Dependence of R_h (open symbols) and $\delta R_h/R_h$ (closed symbols) of PEGylated nanogels on pH: CD1 (circles), CD2 (triangles), and CD5 (squares). A full color version of this figure is available at *Polymer Journal* online.

pH=5.8 was ~90% and that of CD5 was ~80%. From the pH-α curves, the pK_a values of CD1, CD2 and CD5 were evaluated to be 6.9, 6.9 and 6.6, respectively; the results show that the pK_a values of the nanogels slightly shifted toward an acidic pH with the increase in the cross-link density of the core.

Increase in nanogel size upon pH change

The pH dependence of R_h and $\delta R_h/R_h$ on the cross-link density of the PEGylated nanogel is shown in Figure 2. The values of R_h drastically changed around the pK_a of each sample; the sizes of PEGylated nanogel particles increased at a pH level lower than the pK_a. This tendency is consistent with a previous DLS measurement of similar nanogel particles.[22] The values of R_h at a higher pH were ~40 nm regardless of their cross-link density, whereas those at a lower pH decreased with the increase in cross-link density. This result indicates that the cross-link density of the core affects the increase in nanogel size.

Results of SAXS measurement

Figure 3 shows the SAXS intensity profiles of the PEGylated nanogels and their corresponding fitting curves at pH 5.8. and pH 8.0. Several

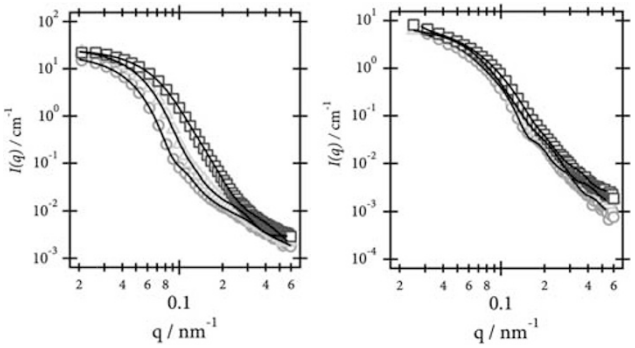

Figure 3 SAXS intensity profiles of CD1, CD2, and CD5 at pH 5.8 (left) and pH 8.0 (right): CD1 (circles), CD2 (triangles), and CD5 (squares). The lines show fitting curves. A full color version of this figure is available at *Polymer Journal* online.

shoulders are recognized in the intensity profiles, although their shape is not clear. This result indicates that the size and shape of the PEGylated nanogels were moderately monodispersed and that the PEGylated nanogels show a sphere-like structure. At pH 8.0, the scattering intensity profiles are almost identical to each other, whereas, at pH 5.8, they are significantly different. A comparison of the intensity profiles shows that CD1 and CD2 increase in size upon a change in pH from 8.0 to 5.8 compared with CD5; these results support the above-mentioned DLS results.

To obtain more detailed structural information, we fitted the SAXS intensity profiles by employing several kinds of structural models and found that a concentric core-shell sphere model provides the best-fit curve. The function describing concentric core-shell spheres is as follows:

$$I(q) = Nr_e^2[\Delta\rho_c V_c F(q, R_c) + \Delta\rho_s V_{total} F(q, R_{total})]^2,$$

where N is the number of spheres and r_e is the classical electron radius. $\Delta\rho_c$ and $\Delta\rho_s$ represent the contrast in electron density between the core and the shell and that between the shell and solvent, respectively. The sizes of the core and shell are defined by the radius of the core R_c and that of the entire particle R_{total}. V_c and V_{total} are the volume of the core and the entire particle, respectively. $F(q)$ is the form factor of a sphere, which is described by the following equation:

$$F(q, r) = \frac{3[\sin(qr) - qr\cos(qr)]}{(qr)^3}.$$

The polydispersity of nanogel particles is taken into account by assuming that the core volume has a Gaussian distribution, whose variance is evaluated with the standard deviation of the particle radius, δR_c. In this study, the scattering contrast of the shell, $\Delta\rho_s$, is much smaller than that of the core, $\Delta\rho_c$; thus, the assumption that only the core size is polydispersed is guaranteed when interpreting the present scattering intensity profiles. The fitting curves agree well with the experimental data, indicating that the present core-shell model is fairly reasonable.

Swelling behavior of core upon pH change

The fitted values of R_c and $\delta R_c/R_c$ are shown in Figure 4. The radius of the core, R_c, increases upon a change in pH from 8.0 to 5.8, for all the samples, although the increase in the radius of CD5 is much smaller than that of the other gels; this result indicates that the core of a PEGylated nanogel is swollen upon a change in pH. The origin of this swelling behavior is reasonably attributed to the protonation of the core as follows. According to the titration measurement (Figure 1), the

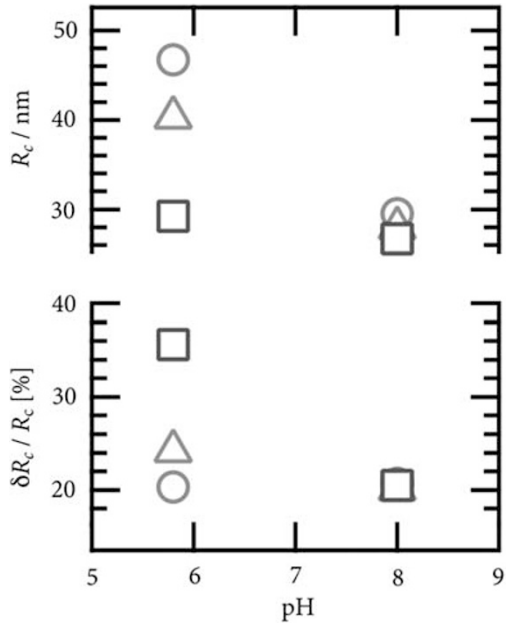

Figure 4 Dependence of R_c (upper) and $\delta R_c/R_c$ (lower) on pH: CD1 (circles), CD2 (triangles), and CD5 (squares). A full color version of this figure is available at *Polymer Journal* online.

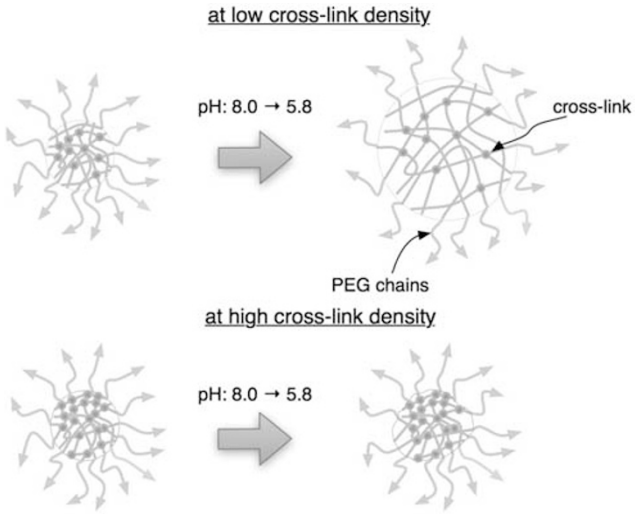

Figure 5 Schematic view of swelling behavior of a PEGylated nanogel. When the cross-link density is low (CD1), the number of cross-links is small; thus, the swelling develops rather homogeneously. When the cross-link density is high (CD5), the number of cross-links is large, which results in an inhomogeneous deformation of the nanogel. A full color version of this figure is available at *Polymer Journal* online.

nitrogen atoms of DEAMA in the core were not protonated under alkaline conditions (pH 8.0). By contrast, most of the nitrogen atoms in the core were protonated under acidic conditions (pH 5.8) by the influx of H^+ ions; the ions may have attached themselves to an amine group of DEAMA. Thus, the electrostatic repulsion in the cores at pH 5.8 increases compared with that at pH 8.0 for all of the cross-link densities. This increase in electrostatic repulsion may be a dominant driving force of the swelling of the core upon a change in pH.

Figure 4 shows that the degree of the size-increase highly depends on the cross-link density; the core size at pH 5.8 increases as the cross-link density decreases. This tendency is somewhat peculiar when one recalls the fact that the number of nitrogen atoms that functions as a source of repulsive forces is similar over the entire sample. The results of titration measurements (Figure 1) indicate that most of the nitrogen atoms were protonated at pH 5.8; thus, the repulsive force due to the protonation should be on the same order. It should be noted that counter ions such as Cl^- neutralize the effect of protonation to a certain extent and that this might depend on the cross-link density; nevertheless, the above discussion holds qualitatively. The discrepancy between the core sizes of the samples with the different cross-link densities is reasonably explained by considering the competition between repulsive forces (electrostatic repulsion forces) and attractive forces, such as that manifested by the rubber elasticity of core polymers. The force originating from rubber elasticity generally depends on the cross-link density. Let us assume that (i) the number of core polymers, not counting the cross-linker (EGDMA), is constant independent of the cross-link density, (ii) the core of the swollen state is incompressible, and (iii) the interaction between partial chains (the chain between neighboring cross-link) can be ignored; then, the free energy density of elasticity is simply proportional to the number of partial chains. This qualitatively shows that the attractive force, or the force opposing the swelling, increases with the cross-link density. The preceding discussion is purely qualitative and requires further rigorous experimental and theoretical study; thus, we omit the quantitative discussion in the present paper.

It should be noted that the polydispersity of the core size obtained by SAXS measurement (Figure 4, lower panel) is independent of the cross-link density at pH 8.0, while it increases with the increase of cross-link density at pH 5.8. The polydispersity is, in principle, independent of the pH conditions for each specimen, as is the case for $\delta R_h/R_h$ (Figure 2). The change in polydispersity can be explained in terms of the structural inhomogeneity of the core. In CD1, the number of cross-links in the core is relatively small; this causes the region that obstructs homogeneous swelling due to the presence of cross-links to be relatively small. In this case, the swelling is expected to develop homogeneously and the polydispersity of the core size does not change after swelling. In the case of CD5, the number of cross-links in the core is relatively large; the core certainly has regions where swelling develops and regions that do not swell. In this way, the core inhomogeneously swells both in shape and size; as a result, the polydispersity of CD5 greatly increases upon swelling. CD2 has a moderate number of cross-links, and its polydispersity at pH 5.8 is thus an intermediate value between the polydispersities of CD1 and CD5. The dependence of R_c on the cross-link density supports this notion. In CD5, the core size barely changes upon a change in pH from 8.0 to 5.8, while the polydispersity greatly increases; this indicates that tiny parts of the core swell or deform upon a change in pH, whereas the core does not swell as a whole. This results in an inhomogeneous shape and size distribution of the core.

From the above discussion, it can be concluded that the distribution of cross-links is not homogeneous, particularly in CD5. This situation is schematically shown in Figure 5. The inhomogeneous structural distribution of cross-links affects the difference in swelling behavior between CD1, CD2 and CD5 in addition to the competition between the repulsive and attractive forces in the core described previously. This structural model provides a good explanation of the difference between the pH dependence shown by SAXS and DLS. Hydrodynamic radii are estimated from the diffusion behavior of particles in DLS, whereas the actual topological structure can be measured by SAXS. The hydrodynamic radii will be highly affected by the presence of a

shell, and the effect of core polydispersity ($\delta R_c/R_c$) on the polydispersity of the hydrodynamic radius ($\delta R_h/R_h$) will be smeared; thus, the polydispersity of the hydrodynamic radius hardly depends on a change in pH. In the case of CD5, the increase in core polydispersity is likely to increase the associated drag forces in solution, which leads to an increase in the estimated hydrodynamic radius; thus, the hydrodynamic radius increases with a change in pH from 8.0 to 5.8, whereas the core size barely changes.

CONCLUSIONS

In this study, we investigated the structure of PEGylated nanogels with SAXS and DLS. Nanogel cores were observed to swell upon a change from alkaline to acidic pH conditions. A higher cross-link density in the core prevents the nanogel from homogeneously swelling, that is, the core size hardly increases and the polydispersity of the nanogel particle size changes. At a lower cross-link density, the core considerably increases in size upon a change in pH with homogeneous swelling. This swelling behavior may have a key role in the pH-induced controlled release of drugs. Further studies such as the *in situ* observation of drug release from pH-responsive nanogels using time-resolved SAXS will help us to clarify the mechanism of drug release, which will lead to the development of high-performance drug delivery system systems.

ACKNOWLEDGEMENTS

The SAXS experiments were performed under the approval of the SPring-8 Proposal Advisory Committee (2009B1202 and 2009B7200). We appreciate the support of Dr H Masunaga and Dr K Ito (JASRI) when performing the experiments.

1 Ferrari, M. Cancer nanotechnology: opportunities and challenges. *Nat. Rev. Cancer* **5,** 161–171 (2005).
2 Davis, M. E., Chen, Z. G. & Shin, D. M. Nanoparticle therapeutics: an emerging treatment modality for cancer. *Nat. Rev. Drug Discov.* **7,** 771–782 (2008).
3 Torchilin, V. P. Recent advances with liposomes as pharmaceutical carriers. *Nat. Rev. Drug Discov.* **4,** 145–160 (2005).
4 Kataoka, K., Harada, A. & Nagasaki, Y. Block copolymer micelles for drug delivery: design, characterization and biological significance. *Adv. Drug Deliv. Rev.* **47,** 113–131 (2001).
5 Harris, J. M. & Chess, R. B. Effect of PEGylation on pharmaceuticals. *Nat. Rev. Drug Discov.* **2,** 214–221 (2003).
6 Duncan, R. The dawning era of polymer therapeutics. *Nat. Rev. Drug Discov.* **2,** 347–360 (2003).
7 Gref, R., Domb, A., Quellec, P., Blunk, T., Müller, R. H., Verbataz, J. M. & Langer, R. The controlled intravenous delivery of drugs using PEG-coated sterically stabilized nanospheres. *Adv. Drug Deliv. Rev.* **16,** 215–233 (1995).
8 Bontha, S., Kabanov, A. V. & Bronich, T. K. Polymermicelleswithcross-linkedioniccoresfordelivery of anticancer drugs. *J. Control. Release* **114,** 163–174 (2006).
9 Monacelli, R. & Doretti, M. P. Separation of polyoxyethylene glycol in ice creams. *Boll. Lab. Chim. Prov. (Bologna)* **15,** 235–238 (1964).
10 Kataoka, K., Kwon, G. S., Yokoyama, M., Okano, T. & Sakurai, Y. Block copolymer micelles as vehicles for drug delivery. *J. Control. Release* **24,** 119–132 (1993).
11 Maeda, H., Wu, J., Sawa, T., Matsumura, Y. & Hori, K. Tumor vascular permeability and the EPR effect in macromolecular therapeutics: a review. *J. Control. Release* **65,** 271–284 (2000).
12 Matsumura, Y. & Maeda, H. A new concept for macromolecular therapeutics in cancer chemotherapy: Mechanism of tumoritropic accumulation of proteins and the antitumor agent smancs. *Cancer Res.* **46,** 6387–6392 (1986).
13 Gruenberg, J. The endocytic pathway: a mosaic of domains. *Nat. Rev. Mol. Cell Biol.* **2,** 721–730 (2001).
14 Clague, M. J. Molecular aspects of the endocytic pathway. *Biochem. J.* **336,** 271–282 (1998).
15 Mukherjee, S., Ghosh, R. N. & Maxfield, F. R. Endocyosis. *Physiol. Rev.* **77,** 759–803 (1997).
16 Duncan, R. Drug-polymer conjugates: potential for improved chemotherapy. *Anticancer Drugs* **77,** 175–210 (1992).
17 Oishi, M. & Nagasaki, Y. Synthesis, characterization, and biomedical applications of core–shell-type stimuli-responsive nanogels–Nanogel composed of poly[2-(N, N-diethylamino)ethyl methacrylate] core and PEG tethered chains. *React. Funct. Polym.* **67,** 1311–1329 (2007).
18 Hayashi, H., Iijima, M., Kataoka, K. & Nagasaki, Y. pH-sensitive nanogel possessing reactive PEG tethered chains on the surface. *Macromolecules* **37,** 5389–5396 (2004).
19 Oishi, M., Hayashi, H., Iijima, M. & Nagasaki, Y. Endosomal release and intracellular delivery of anticancer drugs using pH-sensitive PEGylated nanogels. *J. Mater. Chem.* **17,** 3720–3725 (2007).
20 Oishi, M. & Nagasaki, Y. Stimuli-responsive smart nanogels for cancer diagnostics and therapy. *Nanomedicine* **5,** 451–468 (2010).
21 Tamura, A., Oishi, M. & Nagasaki, Y. Efficient siRNA delivery based on PEGylated and partially quaternized polyamine nanogels: enhanced gene silencing activity by the cooperative effect of tertiary and quaternary amino groups in the core. *J. Control. Release* **146,** 378–387 (2010).
22 Tamura, A., Oishi, M. & Nagasaki, Y. Enhanced cytoplasmic delivery of siRNA using the stabilized polyion complexes based on PEGylated nanogels bearing cross-linked polyamine structure. *Biomacromolecules* **10,** 1818–1827 (2009).
23 Glatter, O., Sherf, G., Schillen, K. & Brown, W. Characterization of a Poly(ethylene oxide)-Poly(propylene oxide) Triblock Copolymer (EO27-PO39-EO27) in aqueous solution. *Macromolecules* **27,** 6046–6054 (1994).
24 Nakano, M., Deguchi, M., Matsumoto, K., Matsuoka, H. & Yamaoka, H. Self-assembly of Poly(1,1-diethylsilabutane)-block-poly(2-hydroxyethyl methacrylate) block copolymer. 1. Micelle Formation and Micelle-Unimer-Reversed Micelle transition by solvent composition. *Macromolecules* **32,** 7437–7443 (1999).
25 Pedersen, J. S., Svaneborg, C., Almdal, K., Hamley, I. W. & Young, R. N. A small-angle neutron and X-ray contrast variation scattering study of the structure of block copolymer micelles: corona shape and excluded volume interactions. *Macromolecules* **36,** 416–433 (2003).
26 Riley, T., Heald, C. R., Stolnik, S., Garnett, M. C., Illum, L., Davis, S. S., King, S. M., Heenan, R. K., Purkiss, S. C., Barlow, R. J., Gellert, P. R. & Washington, C. Core-shell structure of PLA-PEG nanoparticles used for drug delivery. *Langmuir* **19,** 8428–8435 (2003).
27 Akiba, I., Terada, N., Hashida, S., Sakurai, K., Sato, T., Shiraishi, K., Yokoyama, M., Masunaga, H., Ogawa, H., Ito, K. & Yagi, N. Encapsulation of a hydrophobic drug into a polymer-micelle core explored with synchrotron SAXS. *Langmuir* **26,** 7544–7551 (2010).
28 Tamura, G., Shinohara, Y., Akiba, I., Tamura, A., Oishi, M., Nagasaki, Y., Sakurai, K. & Amemiya, Y. pH-responsive structural change of PEGylated amine-bearing nanogel explored by small angle X-ray scattering. *J. Phys. Conf. Ser.* **272,** 012018 (2011).
29 Berne, B. J. & Pecora, R. *Dynamic Light Scattering with Application to Chemistry, Biology and Physics*, Dover Publications, New York, (2000).
30 Masunaga, H., Ogawa, H., Takano, T., Sasaki, S., Goto, S., Tanaka, T., Seike, T., Takahashi, S., Takeshita, K., Nobuteru, N., Ohashi, H., Ohata, T., Furukawa, Y., Matsushita, T., Ishizawa, Y., Yagi, N., Takata, M., Kitamura, H., Sakurai, K., Tashiro, K., Takahara, A., Amemiya, Y., Horie, K., Takenaka, M., Kanya, T., Jinnai, H., Okuda, H., Akiba, I., Takahashi, I., Yamamoto, K., Hikosaka, M., Sakurai, S., Shinohara, Y., Okada, A. & Sugihara, Y. Multipurpose soft-materials SAXS/WAXS/GISAXS beamline at SPring-8. *Polym. J.* **43,** 471–477 (2011).
31 Fujisawa, T., Inoue, K., Oka, T., Iwamoto, H., Uruga, T., Kumasaka, T., Inoko, Y., Yagi, N., Yamamoto, M. & Ueki, T. Small-angle X-ray scattering station at the SPring-8 RIKEN Beamline. *J. Appl. Cryst.* **33,** 797–800 (2000).
32 Sakuragi, M., Kusuki, S., Hamada, E., Masunaga, H., Ogawa, H., Akiba, I. & Sakurai, K. Supramolecular structures of benzyl amine derivate/DNA complexes explored with synchrotron small angle X-ray scattering at SPring-8. *J. Phys. Conf. Ser.* **184,** 012008 (2009).